28

Application of Wavelets Transform in Rotorcraft UAV's Integrated Navigation System

Lei Dai[1,2], Juntong Qi[1], Chong Wu[1,2] and Jianda Han[1]
[1]*State Key Laboratory of Robotics,*
Shenyang Institute of Automation, Chinese Academy of Sciences
[2]*Graduate School of Chinese Academy of Sciences*
People's Republic of China

1. Introduction

Rotorcraft UAV (RUAV) has similar mechanical structure with helicopter. It can be operated in different flight modes which the fixed-wing UAV is unable to achieve, such as vertical take-off/landing, hovering, lateral flight, pirouette, and bank-to-turn. For these advantages, RUAV can be used in many fields where human intervention is considered difficult or dangerous (Napolitano et al., 1998). So it can perform the tasks such as regional surveillance, aerial mapping, communications relay, power-line inspection, aerial photography and precision load dropping, etc. RUAV has many advantages, such as small in size, low cost, simple operation and convenient transportation. Therefore, RUAV has broad application prospects, high demands, and advantages that the fixed-wing unmanned aircrafts and unmanned airship can not replace.

Integrated navigation system can give the movement information of the carrier, thus every UAV has an integrated navigation system. Because of the limitations of weight, volume, power supply and cost, there is no redundant navigation system in RUAV. RUAV does not have the emergency landing properties of fixed-wing aircrafts or airships in case of failures. Therefore, a failure in any part of a RUAV can be catastrophic. If the failure is not detected, identified and accommodated, the RUAV may crash. The use of wavelet transforms the situation of accurately localizing the characteristics of a signal both in the time and frequency domains, the occurring instants of abnormal status of a sensor in the output signal can be identified by the multi-scale representation of the signal (Dabechies, 1988; Isermann, 1984; Zhang, 2000). Once the instants are detected, the distribution differences of the signal energy on all decomposed wavelet scales of the signal before and after the instants are used to claim and classify the sensor faults.

In low cost and small size integrated navigation system, MEMS (Micro Electronic Mechanical System) inertial sensors are used widely. But MEMS inertial sensors, especially MEMS gyroscopes have large noise. It affects the calculation accuracy of angle rotation matrix, and will further affect calculation accuracy of other navigation data such as position, velocity, and angular velocity. In order to improve the calculation precision of position and angle, digital filter is required to reduce the noise of gyroscope. Commonly, we used

Kalman filters to decreasing the random noise. And we need to build the mathematic model of sensors' errors. The MEMS gyroscope has random drift characteristics of weak nonlinear, non-stationary, slow time-varying. And it is sensitive to external environments such as vibration and temperature. The result of Kalman filter is often imprecision and even divergence, because of inaccurate drift error model of MEMS gyroscope. Wavelet transform has the characteristics of multi-resolution and time-frequency localization, and we do not need to build the mathematic model of sensor errors. So it is ideal for signal processing and analysis of MEMS gyroscope.

However, Synthetic data simulated by means of a computer using real flight data from ServoHeli-20 and ServoHeli-40 RUAV, which is designed and implemented by Shenyang Institute of Automation, have verified the effectiveness of the proposed method.

The following part of this paper is organized as follows. In Section 2, the fault detection approach based on the wavelet transform is established. The RUAV verification platform is introduced in Section 3. The integrated navigation system and the characteristic of inertial sensor are discussed in Section 4. Real RUAV flight fault detection experiments in manual mode are described and discussed in Section 5, and conclusions are given in Section 6.

2. The RUAV platform

During years of research, we have developed two RUAV platforms. The ServoHeli-20 RUAV platform was designed to be a common experimental platform for control and fault-tolerant related study before 2009 (Qi, et al., 2006). The hardware components were selected with considerations of weight, availability and performance. After that, we miniaturized the hardware and used 40Kg industry helicopter. And we developed ServoHeli-40 RUAV platform. This RUAV platform can be used for control and navigation algorithm verification and experimental payload platform.

2.1 ServoHeli-20 platform

As the basic aircraft of the RUAV system, we chose the small-scaled model helicopter which is available in the market. Such a choice is easy for us to exchange the accessories and reduce the cost (Qi, et al., 2010).

2.1.1 Modified RC helicopter

ServoHeli-20 aerial vehicle is a high quality helicopter which is changed by us using a RC model helicopter operating with a remote controller. The modified system allows the payload of more than 5 kilograms, which is sufficient to carry the whole airborne avionics box and the communication units. The fuselage of the helicopter is constructed with sturdy ABS composite body and the main rotor blades are replaced by heavy-duty carbon fibre reinforced ones to accommodate extra payloads. The vehicle is powered by a 90-class glow plug engine which generates 3.0hp at about 15000 rpm, and practical angular rate ranging from 2,000 to 16,000 rpm. The full length of the fuselage is 1260mm and the full width of it is 160mm. The total height of the helicopter is 410mm, the main rotor is 1600mm and the tail rotor is 260mm.

The overall rotorcraft UAV control system comprises: the aerial vehicle platform, the onboard avionics control system, and the ground monitoring station. The UAV helicopter itself is able to operate with the independent control computer system and onboard sensors.

2.1.2 Navigation sensors

In order to navigate following a desired trajectory while stabilizing the vehicle, the information of helicopter's position, velocity, acceleration, attitude, and the angular rates should be known to the guidance and control system. The ServoHeli-20 RUAV system is equipped with sensors including IMU (Inertial Measure Unit), GPS and digital compass, to obtain above accurate information about the motion of the helicopter in association with environment.

Sensor	PARAMETERS
IMU400 IMU	Angular Rate Range: $\pm 100^{\circ}/\sec$ Acceleration Range: $\pm 4g$ Digital Output Format: RS-232 Update Rate: > 100 Hz Size: 76.2 × 95.3 × 81.3 mm Weight: <640g
Crescent GPS	Position Accuracy (CEP): 1.5m Digital Output Format: RS-232 Update Rate: 10 Hz Size: 71.1 × 49.6 × 1.2 mm Weight: 20g
HMR3000 Compass	Pitch, Roll Angular Range: $\pm 40^{\circ}$ Digital Output Format: RS-232 Update Rate: 20 Hz Size: 15 × 42 × 8.8 mm Weight: 92g

Table 1. Sensors parameters

The picture of sensors in the avionics box is shown in Fig. 1, and their primary parameters are shown in Table I.

2.1.3 Processor and control system

The flight computer installed in avionics box is a typical industrial embedded computer system, so-called PC-104 in the whole system is kept as compact and light-weight as possible. The PC-104 has the ISA or PCI bus which features a $108.2\text{cm} \times 115.06\text{cm}$ footprint circuit board. Our flight computer system consists of a main CPU board and some other peripheral boards such as DC-DC power supply board, 8-channel serial communication device and PWM generation board. The main CPU board has a Celeron processor at 400MHz with 256MB SDRAM, fully compatible with the real-time operation system such as QNX. Hard drive or other equivalent mass-storage device for booting and running an operation system and storing useful sensor data is needed to the flight computer.

To our flight control system, a real-time operation system (RTOS) is required for the onboard computer system. After carefully consideration and comparison, QNX Neutrino RTOS is selected as the operation system, which is ideal for embedded real-time applications. It can be scaled to very small size and provide multitasking threads, priority-driven pre-emptive scheduling, and fast context-switching–all essential ingredients of an embedded real-time system. The applied program can be coded and debugged in the remote windows-host computers and can be executed in the airborne computer system independently, which provides great convenience during the flight experiments without modifying the program in onboard computer.

2.1.4 Implementation

Designing the avionics box and packing the box appropriately under the fuselage of the helicopter are two main tasks to implement of the RUAV system.

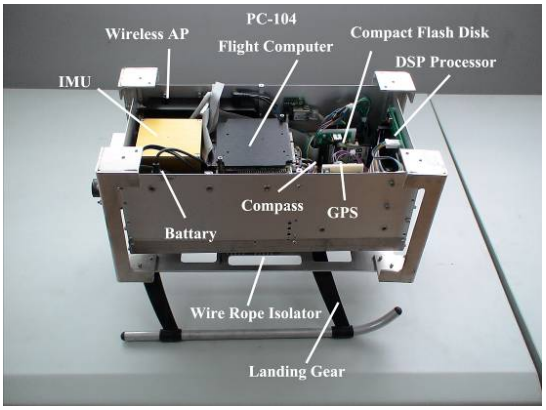

Fig. 1. The avionics control system

In the actual flight environment, the weight and the size of the avionics box are strict limited. Our airborne control box, which is shown in Figure 1, is a compact aluminum alloy package mounted on the landing gear. The center of gravity of the box lies on the IMU device where is not the geometry center of the system that ensure the navigation data form IMU accurate. The digital compass and the IMU are installed on the same line, which are taken as the horizontal center of the gravity of the avionics system to locate and the other components.

The original landing gear of the model helicopter is plastic, in which is no enough room to install the designed avionics system in the fuselage of the helicopter. While, we re-design a landing gear with aluminum alloy and make a larger room under the fuselage of the model helicopter for the control box. To avoid the disciplinary vibration about 20Hz caused by characteristic of the helicopter, ENIDINE® aviation wire rope isolators which are mounted between the avionics box and the changed landing gear are chosen. They are comprised of stainless steel stranded cable, threaded through aluminum alloy retaining bars, crimped and mounted for effective vibration isolation. The assembled RUAV system with the necessary components is shown in Figure 2.

Fig. 2. Implemented ServoHeli-20 RUAV

The full duplex wireless-LAN equipments are installed in the ground station and the airborne system to exchange data between them including receiving commands from the ground system and reporting the operating status or possible damages to the ground station. The architecture of the RUAV control system is presented in Figure 3.

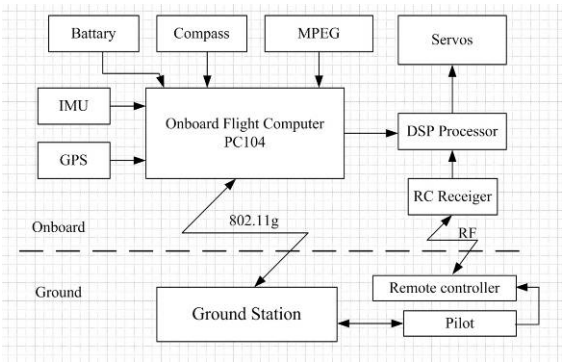

Fig. 3. Architecture of the RUAV control system

2.2 ServoHeli-40 platform

ServoHeli-40 RUAV platform is a flexible platform. It can carry 15Kg payloads to do aerophotography or experiment. It is also easy for us to replace the accessories and the cost is affordable.

2.2.1 ServoHeli-40 helicopter

ServoHeli-40 aerial vehicle is a high reliability helicopter. It uses traditional helicopter configuration of single-rotor with tail rotor. The power is come from 8hp twin-cylinder two-stroke air-cooled gasoline engine. The fuselage of the helicopter is constructed with aluminium. The bearings and the other parts are standard industry parts. So it is easy to buy and repair. ServoHeli-40′s maximum takeoff weight is 40Kg, and its maximum payload is 15 kg. It can carry different kinds of instruments to do experiment. The rotor diameter is

2150 mm. The total height of the helicopter is 770mm, the full width of it is 720mm, and the total length is 2680mm. The maximum airspeed is 100 km/h, and it can cruise 1 hour at 36 km/h speed.

2.2.2 Navigation system

In the design of the navigation system, we followed some principles. First, the system must be compact and easy to equip on the airframe. Second, the system should use low-cost sensor to reduce the RUAV system's cost. Third, the system should be designed as light as possible to save fuel and increase the payload. Precision navigation information of flight state is needed to realize the autonomous control of the RUAV. Generally, navigation information must include positions, velocities, accelerations, attitude, heading and angular velocities in 3-axis. The architecture of the navigation system is shown in Figure 4 (Wu, et al., 2010).

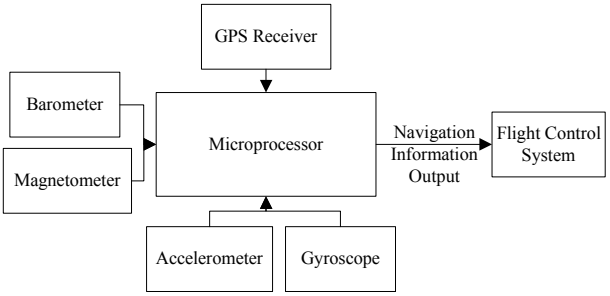

Fig. 4. Hardware Architecture of Navigation System

We use GPS receiver to give position and velocity. But the altitude given by GPS generally has a fluctuation of 5m, and it is not accurate enough to control the RUAV. So a barometer is needed to give a more accurate measurement of the relative altitude. Even though the barometer is more accurate in relative altitude, it is susceptible to weather condition and may vary significantly in different weather. Because the altitude given by GPS is much more unsusceptible to weather, a combination of GPS altitude and barometer altitude will give more accurate and stable altitude information.

Attitudes' accuracy is the key point for the stability of the RUAV since the position control of the RUAV is coupled with the attitude. We use IMU to measure the acceleration and angle velocity. By referring to a low-cost attitude design described in literature (Gao et al., 2006), we determine the attitude in pitch and roll by accelerometers and gyroscopes. A simple calculation of acceleration may be suitable for the RUAV in hovering and other mode with low maneuverability in low acceleration, but in high maneuverability mode with high acceleration, the measurement will deviate a great deal because the measurement of accelerometers include not only gravity acceleration but also absolute acceleration. So a feedback from velocity is added to decrease the influence of absolute acceleration.

The yaw of RUAV will be calculated by the magnetic field measured by the magnetometer. Due to the deviation of magnetic field of the earth in different places, a revision of magnetic field would be necessary to get the real yaw.

Compared with previous generation, this navigation system uses independent processor. We choose LPC3250 as the calculation and acquisition processor. A two-stage EKF is implemented to estimate the flight state. Further research in navigation theory can be conducted by using this system.

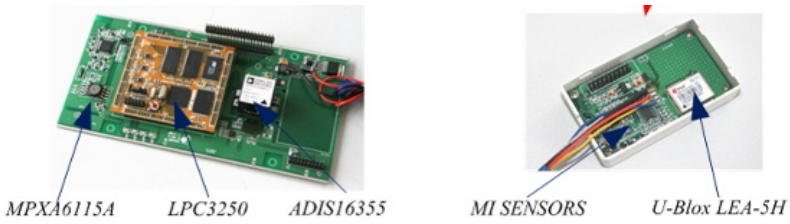

Fig. 5. The navigation system

The IMU, GPS, barometer, magnetometer and processor are integrated in a compact circuit, as shown in Figure 5. The primary parameters of compacted navigation system are shown in Table2.

Sensor	PARAMETERS
ADIS16355 IMU	Angular Rate Range: $\pm 300^{\circ}$ / sec Acceleration Range: $\pm 18g$ Digital Output Format: SPI Update Rate: 50 Hz Size: 23 × 23 ×23mm
U-Blox LEA-5H GPS	Position Accuracy (CEP): 3m Digital Output Format: Uart Update Rate: 4Hz Size: 17 × 22.4 × 3mm
SmartSens Magneto-inductive Compass	Pitch, Roll Angular Range: $\pm 40^{\circ}$ Analog Output Update Rate: 20 Hz
MPXA6115A Barometer	Sensor range: 15 to 115 kPa Analog Output Update Rate: 50 Hz Size: 7.5 × 10 ×10mm

Table 2. Sensors Parameters

2.2.3 Flight control system

The fight control processor uses the same processor as the navigation system, so we can share the code of the operating system and reduce the debug time. The LPC3250 with an ARM926EJ-S CPU Core implementation uses Harvard architecture with a 5-stage pipeline and operates at CPU frequencies up to 266 Hz. The Vector Floating Point (VFP) coprocessor makes the micro controller suitable for advanced navigation and control algorithm, and processing speed and interface versatility is guaranteed. The industry standard operation

temperature from -40℃ to 80℃ extends the usage of RUAV in various environments. The LPC3250 includes a USB 2.0 Full Speed interface, seven UARTs, two I²C interfaces, two SPI/SSP ports, and two I2S interfaces; Such a great number interfaces of LPC3250 makes it very suitable for navigation and control system with a plenty of sensors in standard interface. We designed interface circuit to drive the actuator and log the flight data.

To decrease the developing work in programming, while increasing the system stability, a μC/OS-II embedded system is installed to organize the software development. This small sized embedded system is quite convenient to install; the hard-real-time architecture also makes it suitable for a time critical avionics system in RUAV. We divided the work of software into 5 parts. First, the OS Kernel is to maintain the whole system and arrange the task schedule. Second, the algorithms implements navigation and control theory. Third, the device interface process is to handle the task for sensor data acquire and drive the actuator. Fourth, the user interface carries out the job to display and receive necessary information to the user. Fifth, the log interface is to log the flight data for our experiment. To make sure that the algorithms can be calculated in time, a hardware timer is used instead of the software timer provided by operator system. With a proper design of the software architecture, the system's stability is maintained and the flexibility is also provided for other algorithm implementations.

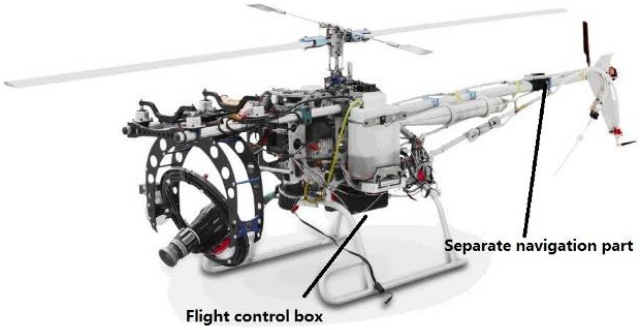

Fig. 6. Implemented ServoHeli-40 RUAV

2.2.4 System realization

The GPS receiver and magnetometer are in a separate part and the others are in the main navigation part. The flight control system and main navigation system are assembled in an anti-jamming aluminum box, and called flight control box. Such a separation is with the consideration that the GPS and magnetometers are susceptible to the install position because they may be influenced if it is covered by the airborne or near some magnetic material. The flight control box is mounted under fuselage of the RUAV. The separate part can be equipped in a proper place on the airframe. To avoid the disciplinary vibration about 20-22.5Hz caused by revolving of main rotor, ENIDINE aviation wire rope isolators are also used. They are comprised of stainless steel stranded cable, threaded through aluminum alloy retaining bars, crimped and mounted for effective vibration isolation. The assembled RUAV system with the necessary components is shown in Figure 6.

To increase the control distance and reliability, the half duplex industry radios are installed in the ground station and the airborne system to exchange data. The data includes commands, operating status and possible damages, which is received and reported to the ground station. The flight data can be logged in SD card, we can analysis the data after flight test. The architecture of the RUAV control system is presented in Figure 7.

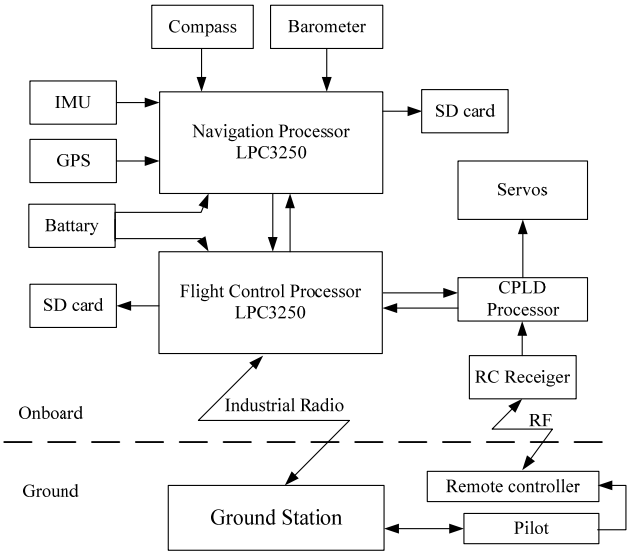

Fig. 7. Architecture of the RUAV control system

3. Wavelet-based fault detection

Without loss of generality, assume that the vehicle's sensor output $y(t)$ is described as (Zhang & Yan, 2001):

$$y(t) = f[x(t)] + n(t) \tag{1}$$

Where $n(t)$ is a noise signal and the measured $x(t)$ changes with a k-degree polynomial function $f[x(t)]$ which describes the measured process changes. Stone-Weierstrass Theorem states that any continuous function on a compact set can be approximated to any degree of accuracy by a polynomial function (Rudin, 1976). Therefore, using a polynomial function to represent any function $f[x(t)]$ will not lose the generality. Let $\psi(t)$ be a wavelet function and $\psi_s(t) = (1/s)\psi(t/s)$ be the dilation of $\psi(t)$ by the scale factor s. The wavelet transform of $y(t)$ can be written as:

$$WT_f(s,\tau) = y(t) * \psi_s(t) = f[x(t) + n(t)] * \psi_s(t) \tag{2}$$

Where $*$ denotes the convolution and $WT_f(s,\tau)$ represents the wavelet transform. A wavelet $\psi(t)$ is said to have m vanishing moments if and only for all positive integers $k<m$, the following equation is satisfied:

$$\int_{-\infty}^{+\infty} t^k \psi_s(t)dt = 0 \tag{3}$$

Now, let us call a smoothing function, any real function $\theta(t)$ such that $\theta(t) = O(1/1(1+t^2))$ and whose integral is nonzero. A smoothing function can be viewed as the impulse response of a low-pass filter. Let $f[x(t)]$ and $\theta_s(t) = (1/s)\theta(t/s)$ be a real function in $L^2(R)$. The abrupt changes of the sensor data at scale s are defined as local sharp variation points $f[x(t)]$ smoothed by $\theta_s(t)$. The method of detecting these sharp variation points with a wavelet transform is explained as follows.

Let $\psi^1(t)$ and $\psi^2(t)$ be the two wavelets defined by:

$$\psi^1(t) = \frac{d\theta(t)}{dt} \tag{4}$$

$$\psi^2(t) = \frac{d\theta^2(t)}{dt^2} \tag{5}$$

The wavelet transform defined with respect to each of these wavelets are given by:

$$W^1(t) = f * \psi_s^1(t) = f * (s\frac{d\theta_s}{dt})(t) = s\frac{d}{dt}(f * \theta_s)(t) \tag{6}$$

$$W^1(t) = f * \psi_s^1(t) = f * (s\frac{d\theta_s}{dt})(t) = s\frac{d}{dt}(f * \theta_s)(t) \tag{7}$$

The wavelet transforms of $W^1 f(s,t)$ and $W^2 f(s,t)$ is proportional respectively to the first and second derivatives of $f[x(t)]$ smoothed by $\theta_s(t)$. As a result, the local maxima of $|W^1 f(s,t)|$ indicate the locations of sharp variation points and singularities of $f[x(t)] * \theta_s(t)$ (Mallat & Hwang, 1992).

From (4) to (7), it can be concluded that the wavelet transform of the signal (1) only includes some sharp variation points induced by sensor faults and random noise. Once a sharp variation point is claimed, and alarm will be triggered for a failure of the sensor.

4. Fault detection experiment

4.1 Fault detection system design

The sensors of the navigation system with different mechanism also have different performance. We cannot get the ideal fault detection results using the traditional fault detection techniques.

In order to accompany the short control period and the highly update rate, we use the parallel wavelet analyzer, which is shown as figure 8.

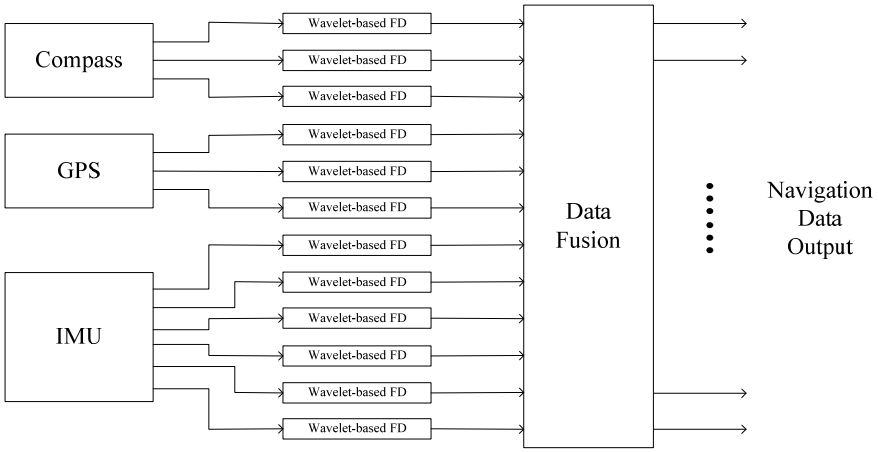

Fig. 8. Architecture of wavelet-based sensor system

Table 1 shows us that there are three sensors in the RUAV sensor system which have three channel separately. We design 12 wavelet analyzers for 12 channels of all sensors. The sensors data will directly send to the data fusion system when the data are in the normal states. However, if the sensors data is abnormal in one or some channels as a result of the failure of specific sensors, the alarms will send to the flight computer while the data link will be cut off. Then the navigation system will continue to compute with degraded sensors data.

4.2 Experimental results and discussion

The proposed wavelet-based fault detection system tested using the ServoHeli-20 RUAV system in manual mode.

Fig. 9. ServoHeli-20 fault detection experiment

The use of the mathematical model makes it easier to test the wavelet-based fault detection system, but the characteristic of the datasets may not reflect the real flight environment and the actual actuator failures. On the other hand, real autonomous flight experiments with an injected sensor failure can be potentially dangerous for the helicopter because it can take the RUAV out of control and RUAV may crash. Thus, we planned to inject the sensor failure while the absence of the security problems of the RUAV with its manual mode. As is shown in the figure 9, the pilot controls the helicopter using radio controller. The onboard computer online detects the fault with wavelet-based algorithm (Qi & Han, 2007).

To demonstrate the effectiveness of the fault detection scheme, the failure scenario of abrupt bias and spike in compass roll channel is assumed.

A "db2" ("db" is define in Matlab) wavelet with a vanishing moment 2 is applied to these abrupt faults of sensor. Figure 10 and 11 show their wavelet transforms in scale-D1 to scale-S3 including the original data signals. In figure 10, scale-D1 to scale-D3 denote the details of the wavelet transform of the signals on scales 1 to 3, respectively, while the scale-S3 represents the approximation of them on scale 3.

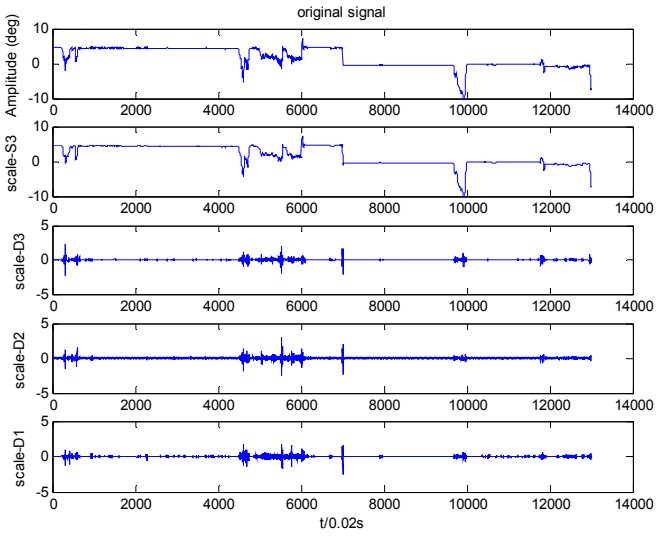

Fig. 10. Bias failure and its wavelet transform(t=0.02s)

4.2.1 Failure of bias

In figure 10, an example sensor failure experiment is presented. At the point of 7000, the compass roll channel gets bias of 5 degree.

The local maxima of the first derivative are sharp variation points of $f[x(t)]*\theta_s(t)$. For abrupt failure detection, we are only interested in the local maxima of $|W^1 f(s,t)|$. When detecting the local maxima of $|W^1 f(s,t)|$, we call also keep the value of the wavelet transform at the corresponding location.

As is shown in the figure 11, discontinuity point of signal is displayed obviously, it is allocated very accurately in time-domain, and fault point of bias signal is contained in signal abruption. Using the $|W^1 f(s,t)|$ criterion, the fault detection system can detect locations of the bias fault at 7000 that we can see the local maximum value of module indicates the signal singularity accurately.

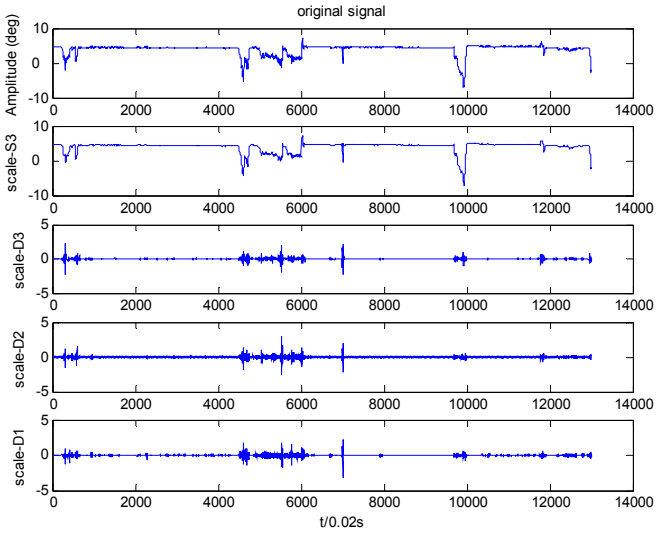

Fig. 11. Spike failure and its wavelet transform(t=0.02s)

4.2.2 Failure of spike

We also made a spike failure injection to RUAV system in manual mode to test the performance of the wavelet-based fault detection system. At the point of 7000, the compass roll channel gets spike which the signal return to zero.

Similar to the bias failure experiment, the location of fault agree with the maximum values of the wavelet transform on different scales.

From the results, it can be conclude that the proposed method is effective for detection the abrupt faults of the RUAV sensor system. Fault point could be also being described accurately at some certain resolution. Local characteristics of wavelet are represented well in time and frequency-domains.

5. Wavelet for gyroscope de-noising

5.1 MEMS gyroscope signal analysis

With the development of microelectronics technology, low cost MEMS gyroscopes begin to be used widely. It makes the great development of integrated navigation system, especially in UAV system. Compared with high costs gyroscope, the MEMS gyroscope devices have

some drawbacks, such as large bias stability, big temperature noise, high noise density. And all these disadvantages lead to that the long-term accuracy of navigation system is very low. While random vibration due to main rotor of RUAV, have an impact on gyroscopes measurements. Simple passive vibration damping measures cannot be completely filtering the vibration. And the measurement error is unacceptable (Ma et al., 2007). In order to eliminate noise of MEMS gyroscope, error analysis of signals need to be done. This is very important to improve the performance of integrated navigation system and increase the stability of the RUAV system.

According to the frequency spectrum characteristics of MEMS gyroscope, its errors can be divided into long-term errors and short-term errors. Long-term errors include bias stability, scale non-linearity, angular random walk, bias variation over temperature, rate noise density, and so on. These errors can be predicted by the mathematic model and adjusted. According to the error mechanism of MEMS gyroscope, an ARMA model is established. Then, using parameter identification, the parameter of the ARMA model is identified. So the long-term errors can be compensated. The short-term errors include random interference noise, measurement noise, and so on. It is a tricky problem to deal with errors. Usually, we use digital filters to compensate the error. These conventional denoising methods include Low-Pass filter, Kalman filter, and wavelet filter. Under the principle of linear least mean squares error, angular velocity estimation is recursively calculated by Kalman filtering in literature (Shi & Zhang, 2000). Although the approach is successfully used in reducing gyroscope noise on the stationary platforms, it is based on the assumption that the signal is corrupted by Gaussian noise and model is exactitude. Unfortunately, for imprecise model and colored noise, this method may yield worse results. Low-Pass filter passes low-frequency signals but reduces the amplitude of signals with frequencies higher than the cutoff frequency. And greater accuracy in approximation requires a longer delay. It can be realized by cheap hardware, while its low quality, however, is not very satisfactory. Wavelet transforms have excellent multi-resolution analysis feature and do not need model. So it is suitable for non-stationary signals processing. And wavelet transforms have been successfully applied to the denoising of signals or images in recent years. This method has achieved good results in gyroscope signal denoising process (Imola et al., 2001; Qu et al., 2009).

5.2 Wavelet for denoising

Wavelet transform is method of time-frequency localization analysis. Its window size (area) is fixed, but the shape can be changed. Wavelet transform developed the short - time Fourier transform of localized. It has a high frequency resolution and lower time resolution in low frequency part of the signal. And in high frequency part of the signal, it has a high time resolution and lower frequency resolution. Wavelet transform method has the character of frequency analysis, and it can indicate the occurred time. It is very suitable for noise reduction of MEMS gyroscopes.

The discrete wavelet function $\psi_{j,k}(t)$ in Discrete Wavelet transform (DWT) can be expressed as :

$$\psi_{j,k}(t) = s_0^{-j/2}\psi\left(\frac{t - ks_0^j\tau_0}{s_0^j}\right) = s_0^{-j/2}\psi\left(s_0^{-j}t - k\tau_0\right) \tag{8}$$

The discrete wavelet translate factor can be expressed as :

$$C_{j,k} = \int_{-\infty}^{\infty} f(t)\psi^*_{j,k}(t)dt = \left\langle f, \psi_{j,k} \right\rangle \tag{9}$$

The reconstruction function of Discrete Wavelet transform can be expressed as :

$$f(t) = C\sum_{-\infty}^{\infty}\sum_{-\infty}^{\infty} C_{j,k}\psi_{j,k}(t) \tag{10}$$

Where s denotes the scale factor, τ denotes the translate factor. The $f(t)$ represents the signal function.

The purpose of wavelet transform for denoising is to extract useful signal and remove the interference signal in the output signal. In other words, the useful signal and noise signal are separated by the method of wavelet transform. There are 4 common methods of wavelet denoising (Burrus et al., 1998; Guo et al., 2003):

1. Thresholding Denoising Method. It is also called wavelet shrinkage. The basic idea of this method can be described as: The wavelet coefficients have different characters in particular wavelet scales. According to this characteristic of the signal and noise, the noise signals are converted by wavelet transform in certain wavelet scales. According to a certain threshold processing strategies for treatment of wavelet coefficients, the coefficients, which are greater than the threshold, are kept (hard thresholding method) or shrunk (soft thresholding method). The coefficients, which are less than the threshold, are considered to be noise and set to zero directly. Then based on these wavelet coefficients, the original signal is reconstructed using inverse wavelet transform. And this method requires the assumption that the noise signal is Gaussian white noise.
2. Wavelet Decomposition and Reconstruction Method. It is also known as the Mallet method. It decomposes the signal with noise in scale into different frequency bands, sets the bands with noise to zero and reconstructs the signal using wavelet method. This method will remove the noise signals with the useful signals. So it may distort the reconstructed signal.
3. Modulus Maximum Method. In different wavelet scale, this method uses the variation features of wavelet transform modulus' maxima value to denoising the signal. The extreme points, whose amplitude decrease with scale increasing in signal, are removed. The extreme points, whose amplitude increase with scale increasing in signal, are retained. Using alternating projection method, the original signal is reconstructed from de-noised diagram of maxima modulus. And the noise signal is de-noised.
4. Translation Invariant Method. It is a method improved from the basis of the Thresholding Denoising method. The noise signals are taken n times cycles shift by this method. And the translated signals are de-noised using thresholding denoising method. In the end, de-noised signal are equilibrated. This method has a smaller mean square error and improves signal-to-noise ratio.

5.3 Thresholding denoising method

Through the above analysis, the modulus maximum method and translation invariant method have large calculation amounts. And this will affect the real-time calculation of integrated navigation system. So considering the speed of calculation and the ease of implementation, thresholding denoising method is used in our navigation system.

The step of thresholding denoising method is as follows (Song et al., 2009; Su & Zhou, 2009):

1. Selecting the Wavelet function. Then the signal with noise $y_i, i = 0,1,...,N-1$ is discrete using wavelet transformation. A group of wavelet transform coefficients $d_{j,k}$ is got. The subscript j is the wavelet scale.
2. Thresholding the wavelet transforms coefficients $d_{j,k}$. The hard threshold, soft threshold or other threshold method can be used to deal with the coefficients. After the computation, a new wavelet transforms coefficients $\hat{d}_{j,k}$ is got.

The hard threshold estimation is defined as follows:

$$\hat{d}_{j,k} = \begin{cases} d_{j,k}, & |d_{j,k}| \geq \lambda_j \\ 0, & |d_{j,k}| < \lambda_j \end{cases} \tag{11}$$

The soft threshold estimation is defined as follows:

$$\hat{d}_{j,k} = \begin{cases} \operatorname{sgn}(d_{j,k})(|d_{j,k}| - \lambda_j), & |d_{j,k}| \geq \lambda_j \\ 0, & |d_{j,k}| < \lambda_j \end{cases} \tag{12}$$

Where λ_j is the threshold constant.

3. Wavelet reconstruction. Using the inverse of discrete wavelet transform formulas, we can get the de-noised signal $\hat{y}_i$.

6. Gyroscope denoising simulation and analysis

In this section, several control experiments are taken on gyroscope signal denoising using wavelet methods. The experiment uses the real flight data recorded by the flight control system of ServoHeli-40. The flight data is recorded at the 100Hz rate, and each point represents 10ms. It is sufficient to describe the motion of ServoHeli-40 RUAV both in time domain and in frequency domain.

In this simulation experiment, the length of the data is 14,950 points. And it means the data continued about 2.5 minutes. During this period of time, the RUAV did the following actions: standing still, engine ignition, speed idle, hovering , and trajectory tracking. In these flying modes, the data of gyroscope have different amplitude characters. This reflects the vibration differences in different flying modes. The original signal of ServoHeli-40's Y axis gyroscope is shown in the figure 12.

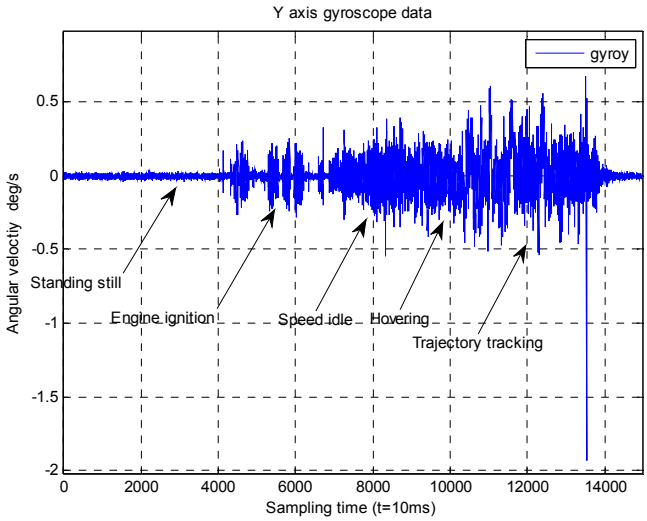

Fig. 12. The original signal of ServoHeli-40's Y axis gyroscope

In order to find a appropriate wavelet functions and decomposition levels, the simulation compared the thresholding denoising method using harr, db2, db4, db6, sym2, sym4, coif2, bior1.5 and bior5.5 wavelet functions. The decomposition levels are respectively 2, 5 and 8. The standard deviation of de-noised signal's residuals is calculated to compare the wavelet denoising results. The results are shown in Table 3. And the standard deviation of the original data is 0.06606.

wavelet / Level	haar	db2	db4	db6	sym2	sym4	coif2	bior1.5	bior5.5
2	0.01841	0.1378	0.01323	0.01285	0.01378	0.01329	0.01288	0.01906	0.01271
5	0.04229	0.05397	0.05467	0.05489	0.05397	0.05561	0.05558	0.05514	0.05572
8	0.06552	0.06537	0.06576	0.0658	0.06573	0.06578	0.06582	0.06573	0.06583

Table 3. Standard deviation of de-noised signal's residuals

In Table 3, when decomposition level increases to more than 5 layers, improvement in de-noised signal's residuals is unobvious. When the de-noised signal's residuals approach to 0.06606, the de-noised signal is close to straight line. And the computation cost is increased as layers increasing. So decomposition level of 5 is a good choice.

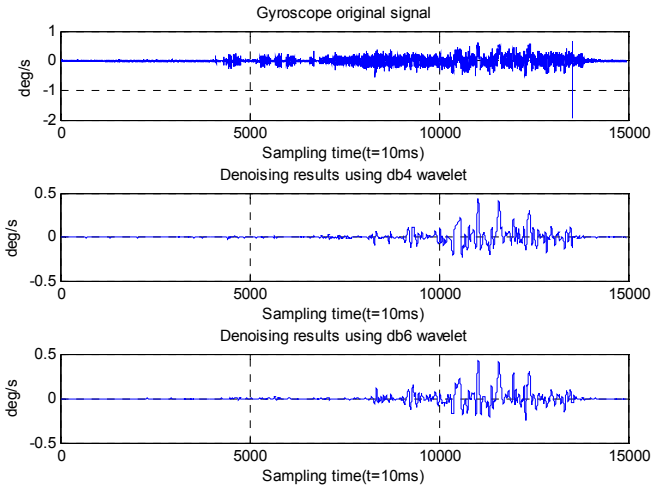

Fig. 13. Contrast of denoised signal and original signal

According to the simulation results, db4, db6 and bior5.5 may be good choice for wavelet functions, because the curve of these de-noised signal are smoother than the others. But bior5.5 have lager computation cost, it is not suitable for real time computation. In Figure 13, the de-noised signals of db4, db6 are compared with the original signal. The denoising result, got from db6 wavelet function, is smoother than the result of db4. And the de-noised signal of db6 is closer to the real angular moment of RUAV than the original signal.

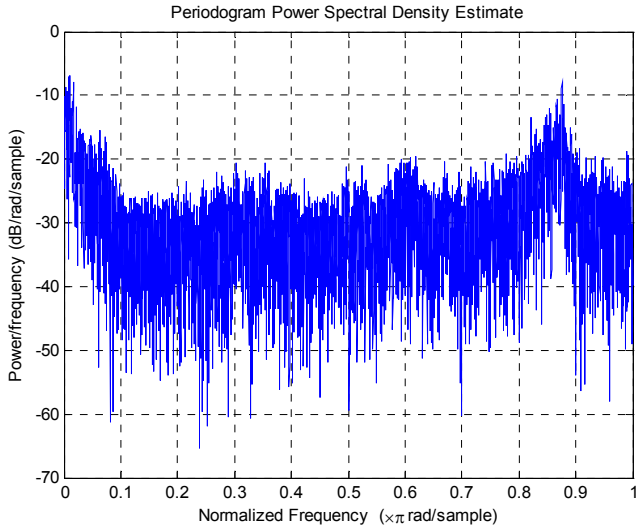

Fig. 14. The periodogram power spectral density estimate of original signal

The periodogram power spectral density estimate of original gyroscope signal is shown in Figure 14. The normalized frequency is 50Hz in this diagram. At 0.87(about 37Hz), the signal has a gain of -10db. In ServoHeli-40 RUAV system, there is a 16.7-45Hz vibration band. This vibration is caused by the rotation of main rotor, engine and tail rotor. 37Hz signal is in this noise band, and it is need to be eliminated.

For the characters of the control system, actuator system, and airframe of helicopter, the motion response of ServoHeli-40 is no more than 3Hz. The vibration frequency larger than 3Hz is out of the control of flight control system. Using the denoising result of db6 wavelet function, the spectrum energy density is analyzed. The periodogram power spectral density estimate of de-noised signal is shown in Figure 15. In this diagram, the noise signal more than 2.5Hz are eliminated by the algorithm. The wavelet filter can just remove high frequency noise. The denoising results reflected the actual movement of the aircraft. This method is suitable for denoising the noise of gyroscope.

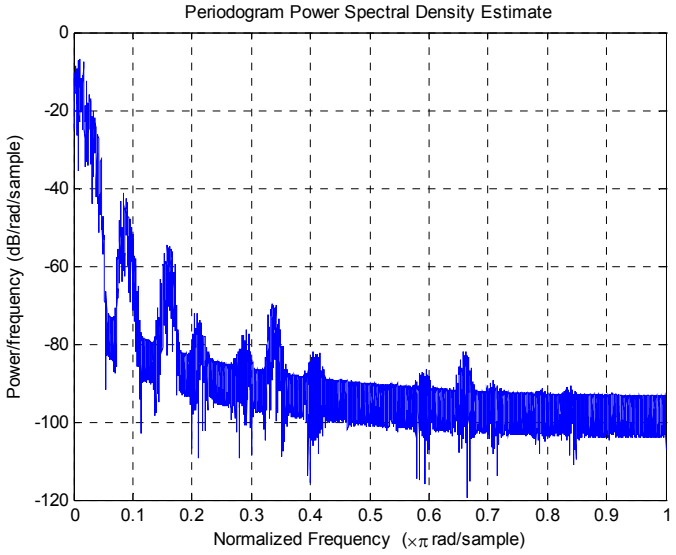

Fig. 15. The periodogram power spectral density estimate of denoised signal using db6 wavelet function

7. Conclusion

In this chapter, wavelet-based algorithm is applied to fault diagnosis and gyroscope noise reduction. Its advantage is that it does not require a prior model of a sensor. The proposed wavelet-based algorithm for fault detection of the RUAV sensor system gives us a multi-scale analysis approach to identify the feature of flight data failures, which are not readily identified by traditional approaches. The results presented in this chapter have shown that

the method based on wavelet transform is a promising alternative to other approaches to the fault detection system for RUAV system. With the wavelet-based scheme, the RUAV sensor fault detection system can detect the failure locations of abrupt signal effectively. In order to overcome the drawbacks of the low-pass filter, the thresholding denoising method base on wavelet transformation is used to reduce the short-term measured noise of the MEMS gyroscope. The article compared different wavelet functions and level of decompositions, and found the effective filter parameters. Using db6 wavelet function at level 5, the de-noised signal is suitable for integrated navigation system and flight control system. This will improve the calculation precision of angle rotation matrix, and the high frequency noise will be decrease.

In the Further, further flight tests are needed to verify the actual performance of wavelet-based denoising method and wavelet-based fault detection in ServoHeli-40's integrated navigation system.

8. Acknowledgments

This work was partially supported by the National Natural Science Foundation of China, "A novel method about the flight control for flying-robot, based on the characteristics of human's brain decision" (No.61005086). And the authors gratefully acknowledge the contribution of Shenyang Institute of Automation, Chinese Academy of Sciences and reviewers' comments.

9. References

Burrus C. Sidney, Gopinath Ramesh A, Guo Haitao. (1998). *Introduction to Wavelets and Wavelet Transforms: A Primer*. Prentice Hall, Inc, 0134896009, New Jersey.

Daubechies Ingrid. (1988). Orthonormal bases of compactly supported wavelets. *Communications on Pure Applied Mathematics*, Vol.41, No.7, (October 1988), pp.(909–996), 10.1002/cpa.3160410705.

Gao Tongyue, Gong Zhenbang, Luo Jun, Ding wei, Feng wei. (2006). An Attitude Determination System For A Small Unmanned Helicopter Using Low-Cost Sensors. *Proceedings of the 2006 IEEE International Conference on Robotics and Biomimetics, 1-4244-0570-X*, Kuming China, December 2006.

Guo Jiang-chang, Teng Jian-fu, Zhang Ya-qi. (2003). The denosing of gyro signals by bi-orthogonal wavelet transform. *IEEE Canadian Conference on Electrical and Computer Engineering*, 0-7803-7781-8, Montreal, Canadian, May 2003.

Imola. K. Fodor, Chandrika Kamath, Rika Kamath. (2001). Denoising through wavelet shrinkage: An empirical study. *J. Electron. Imaging*, Vol. 12, No.1,(2003), pp. (151 – 160), 10.1117/1.1525793.

Isermann Rolf. (1984). Process fault detection based on modeling and estimation methods—A survey. *Automatica*, Vol.20, No.4, (1984), pp. (387–404), 10.1016/0005-1098(84)90098-0

Ma Jianjun, Zheng Zhiqiang, Wu Mei-ping. (2007). Spectral analysis and denoising of MIMU raw measurement. *Optics and Precision Engineering*, Vol.15, No.2, (February 2007), pp. (261-266), 10042924X(2007) 0220261206.

Mallat S, Hwang W L. (1992). Singularity detection and processing with wavelets. *IEEE Transactions on Information Theory*, Vol.38, No.2, (March 1992), pp. (617–643). 0018-9448

Napolitano M R, Windon D A, Casanova J L, Innocenti M, Silvestri G. (1998). Kalman filters and neural-network schemes for sensor validation in flight control systems. *IEEE Transactions on Control System Technology*, Vol.6, No.5, (September 1998), pp.(596–611), 1063-6536.

Qi Juntong, Han Jianda. (2007). Application of Wavelets Transform to Fault Detection in Rotorcraft uav sensor failure. *Journal of Bionic Engineering,* Vol.4, No.4, (December 2007) pp.265-270, 10.1016/S1672-6529(07)60040-7.

Qi Juntong, Song Dalei, Dai lei, Han Jianda. (2010). The ServoHeli-20 rotorcraft UAV project. *International Journal of Intelligent Systems Technologies and Applications*, Vol.8, No.1-4, (2010) pp.(57-69), 10.1504/IJISTA.2010.030190.

Qi Juntong, Zhao Xinggang, Jiang Zhe, Han Jianda. (2006). Design and implement of a rotorcraft UAV testbed. *IEEE International Conference on Robotics and Biomimetics*, 1-4244-0571-8/06, Kunming, China, December 2006.

Qu Guofu, Zhao Fan, Liu Guizhong, Liu Hongzhao. (2009). Adaptive MEMS Gyroscope Denoising Method Based on the à Trous WaveletTransform. *The Ninth International Conference on Electronic Measurement & Instruments*, 978-1-4244-3864-8/09, Beijing, China, February 2009.

Rudin W. (1976). *Principles of Mathematical Analysis* (Third), McGraw-Hill, 007054235X, New York.

Shi Yu, Zhang Xianda. (2000). Kalman-filtering-based angular velocity estimation using infrared attitude information of spacecraft. *Optics and Precision Engineering*, Vol.39, No.2, (February 2000), pp. (551-557), 10.1117/1.602394.

Song Lijun, Qin Yongyuan,Yang Pengxiang. (2009). Application of Wavelet Threshold Denosing on MEMS Gyro. *Journal of test and measurement technology*, Vol.23, No.1, (April, 2008), pp.(33-36), 1671-7449(2009)01-0033-04.

Su Li, Zhou Xue-mei. (2009). Application of improved wavelet thresholding method for de-nosing gyro signal. *Journal of Chinese Inertial Technology*, Vol.17, No.2, (April 2009), pp.(231-235), 1005-6734(2009)02-0231-05.

Wu Chong, Song Dalei, Dai Lei, Qi Juntong, Han Jianda,Wang Yuechao. (2010). Design and Implementation of a Compact RUAV Navigation System. *IEEE International Conference on Robotics and Biomimetics, 978-1-4244-9319-7,* Tianjing, China, July 2010.

Zhang Jianqiu, Ma Jun, Yan Yong. (2000). Assessing blockage of the sensing line in a differential-pressure flow sensor by using the wavelet transform of its output. *Measurement Science and Technology*, Vol.11, No.3, (March 2000), pp.(178–184),10.1088/0957-0233/11/3/302.

Zhang Jianqiu, Yan Yong. (2001). A wavelet-based approach to abrupt fault detection and diagnosis of sensors. *IEEE Transaction on Instrumentation and Measurement*, Vol. 50, No.5, (October 2001), pp.(1389–1396), 0018-9456.